3 Retrieval of cloud optical thickness and effective radius using multispectral remote sensing and accounting for 3D effects

Hironobu Iwabuchi

3.1 Introduction

Understanding spatial and temporal variations in cloud properties is crucial to determine the radiation balance on Earth. Remote sensing from satellites provides valuable information on cloud physical properties at global scales (e.g., Rossow and Schiffer, 1991). Recent Earth-observing sensors, such as the Moderate Resolution Imaging Spectroradiometer (MODIS) and Global Imager (GLI), have well-designed spectral channels and horizontal resolutions between 250 m and 1000 m. Compared to earlier sensors, these sensors allow improved derivations of atmospheric and land surface properties. Operational products include the cloud optical thickness and effective particle radius, which are very useful for studying aerosols' indirect effects (Radke et al., 1989; Rosenfeld, 2000).

Clouds in the real atmosphere generally exhibit three-dimensional (3D) inhomogeneity. However, clouds have commonly been assumed to be plane-parallel and homogeneous (PPH) in applications that use one-dimensional (1D) radiative transfer theory (e.g., remote sensing). Nakajima and King (1990) developed a two-channel algorithm to retrieve the cloud optical thickness and effective particle radius, using remote measurement data of solar-reflected radiances at visible and near-infrared wavelengths. The same algorithm has been applied to satellite data at regional and global scales (Han et al., 1994; Nakajima and Nakajima, 1995). In the algorithm, observed radiances of individual pixel are compared with 1D radiative transfer calculations. Such retrievals implicitly use the independent pixel approximation (IPA; Cahalan et al., 1994a,b). The IPA method uses 1D radiative transfer theory at local scales; net horizontal transport of radiation is ignored. Of course, real radiative transfer in a cloudy atmosphere is 3D, and 3D radiative effects influence the radiance actually observed from space. Many studies have suggested that cloudy pixels are not independent at the resolution of satellite data, for both visible and near-infrared wavelengths (e.g., Marshak et al., 1995a, 1999, 2006; Chambers et al., 1997; Titov, 1998; Zuidema and Evans, 1998).

If 1D radiation theory is applied to the retrieval of cloud properties, then estimates of cloud parameters are biased because of 3D effects. Not only aver-

age radiance but also amplitude of radiance fluctuation is different from that of the IPA calculation. Thus, statistics of optical thickness retrieved with the IPA are also biased. Several studies have sought to correct the statistics of retrieved optical thickness by accounting for 3D effects (Barker and Liu, 1995; Chambers et al., 1997; Iwabuchi and Hayasaka, 2002). Marshak et al. (2006) investigated theoretically how the 3D effects work on the retrieval of effective radius of cloud droplets and suggested the 3D effects indeed appear in actual observations with MODIS data. At low resolution (e.g., 1 km), information about sub-pixel inhomogeneity in individual pixels cannot be obtained, even though that information is necessary to correctly interpret pixel reflectance. Thus, accurate pixel-by-pixel retrieval cannot be expected from low-resolution data. It is possible, however, to improve conventional IPA retrievals by correcting statistical moments of the retrieved parameters.

A difficulty in remote sensing of inhomogeneous cloud properties arises from the decorrelation between 3D radiances and cloud properties. For example, Fig. 3.1 compares pixel-averaged nadir radiances simulated at visible wavelengths and pixel-averaged cloud optical thickness at 250-m resolution. A strong relationship between IPA radiance and pixel-averaged optical thickness is obvious. Conventional IPA retrieval assumes a one-to-one relationship between the radiative quantity and the physical quantity to be retrieved. However, the 3D radiance (or the observed radiance) is poorly associated with pixel optical thickness. The 3D radiance of every pixel of inhomogeneous clouds is one of multiple solutions of 3D radiative transfer for various spatial arrangements of cloud elements. Regardless, available satellite data are two-dimensional (2D). Satellite-based remote sensing of clouds is clearly an ill-posed problem, and an accurate retrieval should never be expected. A common strategy for this kind of problem is to increase
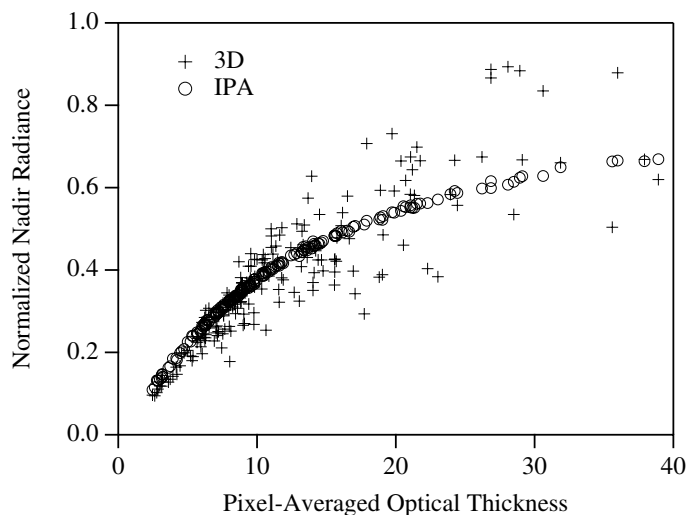

Fig. 3.1. The 3D and IPA radiances as functions of pixel-averaged optical thickness.

the data information used in the retrieval algorithm. To that end, multi-angle, multi-spectral data, which are available from recent Earth-observation sensors, can be used.

If satellite data at high resolution (10–50 m) are available, advanced retrieval methods that include pixel-by-pixel retrieval to account for 3D effects can be used. A fundamental approach to improve retrievals is to base the retrieval model on realistic 3D cloud models and accurate 3D radiation models, rather than on 1D models. Horizontal inhomogeneity in pixels can be ignored for radiances at high resolution, but pixel radiances are greatly influenced by the 3D distribution of cloud elements in the adjacent pixels. Therefore, adjacent pixel information could be used to estimate cloud parameters (Marshak et al., 1998; Oreopoulos et al., 2000; Faure et al., 2002; Iwabuchi and Hayasaka, 2003). For example, if a de-convolution is applied to smoothed data, information lost through radiative diffusion (a 3D effect due to multiple scattering) can be recovered. Marshak et al. (1998) used this technique and proposed an inverse non-local IPA (NIPA) model to retrieve the cloud optical thickness from visible wavelength data. Subsequent demonstrations showed that a similar method could be applied to multi-spectral data to retrieve both optical thickness and effective radius (Faure et al., 2001, 2002; Iwabuchi and Hayasaka, 2003). Zinner et al. (2006) recently applied direct 3D radiative transfer calculations in the optical thickness retrieval algorithm that was based on a standard iteration method. New algorithms using high-resolution data are based on realistic 3D radiative transfer models instead of 1D models, which may increase credibility of the retrieved quantities.

This paper considers the effects of 3D radiative transfer on the retrieval of optical thickness and effective particle radius for boundary layer clouds. Section 3.2 describes the cloud model used to simulate radiances and assess retrieval algorithms. Section 3.3 briefly describes the 3D radiative effects found in the reflected radiances. Such effects are important for understanding 3D artifacts in the retrieved cloud parameters. In Section 3.4, 3D effects in optical thickness retrievals that use 1-km resolution visible reflectance data are discussed. Section 3.5 presents algorithms for pixel-by-pixel retrieval of optical thickness and effective radius; these algorithms account for 3D effects. Section 3.6 includes concluding remarks.

3.2 The stochastic cloud model

Radiances are typically simulated using a 3D radiation model and a model that allows 3D cloud realizations in studies of 3D radiative effects. Realistic assumptions of optical and geometric properties are vital if an accurate retrieval algorithm is to be developed. Cloud/eddy resolving models, observations (e.g., using satellites, cloud radar, or lidar), and artificial stochastic models can provide cloud data. This study uses a stochastic model because it can easily generate cloud distributions with arbitrary cloud parameters. Spectrum-based stochastic models have been used for this purpose (Evans, 1993; Titov, 1998; Iwabuchi and Hayasaka, 2002, 2003). The power spectrum of the cloud optical thickness obeys

the power law $P \sim k^{-\beta}$, where k denotes the wavenumber, and the spectral exponent β is approximately 1.5, yielding values similar to those in observations of stratocumulus clouds (e.g., Barker and Davies, 1992; Davis et al., 1997; Oreopoulos et al., 2000). The scaling exponent is not a dominant parameter for 3D radiation if the exponent is in the range of observed values (Davis et al., 1997; Iwabuchi and Hayasaka, 2002).

Past studies have suggested that the frequency distribution of optical thickness is not Gaussian but has a positive skew (Hayasaka et al., 1994; Cahalan et al., 1994a; Oreopoulos and Davies, 1998b). If the frequency distribution of optical thickness is lognormal, then the probability density function, $p(\tau)$, can be represented as

$$p(\tau) = \frac{1}{\sqrt{2\pi V}\,\tau \ln 10}\, \exp\left[-\frac{1}{2}\frac{(\log \tau - M)^2}{V}\right],\qquad (3.1)$$

where M and V denote the mean and variance of $\log \tau$, respectively. The mean and variance of optical thickness, $\bar{\tau}$ and σ_τ^2, can be determined from M and V in analytic form:

$$\log \bar{\tau} = M + \frac{\ln 10}{2}V \qquad (3.2a)$$

$$\rho_\tau \equiv \frac{\sigma_\tau}{\bar{\tau}} = \sqrt{\exp\left[(\ln 10)^2\, V\right] - 1} \qquad (3.2b)$$

where ρ_τ is the inhomogeneity parameter (a measure of the degree of horizontal inhomogeneity) presented by Davis et al. (1997) and Szczap et al. (2000). Thus, ρ_τ has a one-to-one relation with V when the frequency distribution of optical thickness is lognormal. Analyses of six years of satellite data over northeastern Asian seas revealed variability in the inhomogeneity parameter with respect to season and geographical region; for boundary layer clouds, $V = 0.001 - 0.15$ in a $9 \times 9\,\mathrm{km}^2$ domain (Iwabuchi, 2000).

The adiabatic cloud assumption (e.g., Brenguiter et al., 2000) suggests that the geometrical thickness h (m) of a cloud column is related to optical thickness as follows:

$$h(x,y) = B\sqrt{\tau(x,y)} \qquad (3.3)$$

where B is a coefficient depending on the cloud type. Minnis et al. (1992) reported that the above proportional relationship could also be derived from satellite observations of marine stratocumulus clouds. Vertical variations in the extinction coefficient and effective droplet radius increase with height, as in the adiabatic parameterization of Brenguiter et al. (2000).

Fig. 3.2 shows one spatial distribution of cloud parameters. There is no orientation to the horizontal distribution of optical thickness; any fluctuations are isotropic, unlike for cloud bands. In the example in Fig. 3.2, the base and top of cloud columns are equally rough. The cloud droplet size is large in regions associated with large optical thickness. The positive correlation between local optical thickness and effective radius is reasonable for boundary layer clouds with few drizzle droplets (Bower et al., 1994).
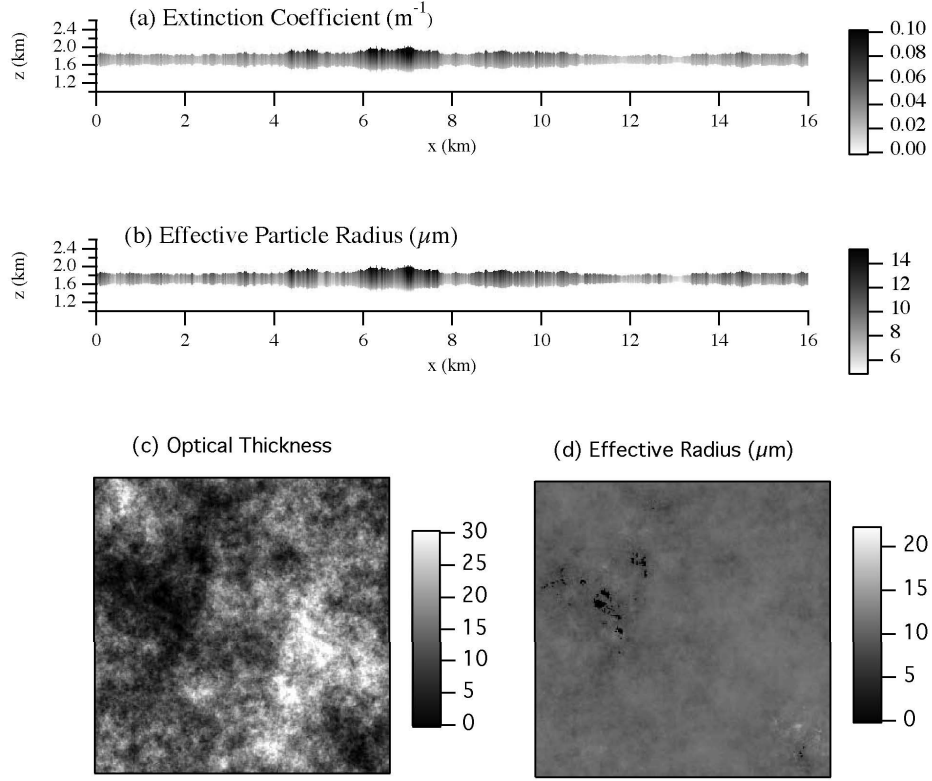
Fig. 3.2. Artificially generated input cloud data: (a) and (b) vertical cross-section of the extinction coefficient at $0.55\,\mu$m wavelength and the effective droplet radius; (c) and (d) as in (a) and (b) but for horizontal distributions.

3.3 Properties of high-resolution radiance

This section describes the 3D effects on high-resolution solar reflected radiance. Differences in the 3D radiance and IPA radiance are important for the inverse problem, as will be shown later. A 3D radiation model that uses Monte Carlo methods was applied to compute solar reflected radiances. The algorithms used in the model have been described by Iwabuchi (2006).

Fig. 3.3 shows horizontal distributions of normalized nadir radiance (reflection function R) from sample computations of 3D radiative transfer (R_{3D}) and IPA (R_{IPA}). The reflection function (normalized radiance) is defined as $R = \pi I/(F_0 \cos\theta_0)$, where I is the radiance, F_0 is the solar irradiance at the top of atmosphere, and θ_0 is the solar zenith angle. The 3D radiance R_{3D} is notably smoother than the IPA radiance R_{IPA} for high solar elevations and rougher for low solar elevations because of smoothing and roughening effects, respectively. These 3D effects have been investigated well by previous studies and known as caused by net horizontal transport of radiation (Marshak et al., 1995a; Várnai
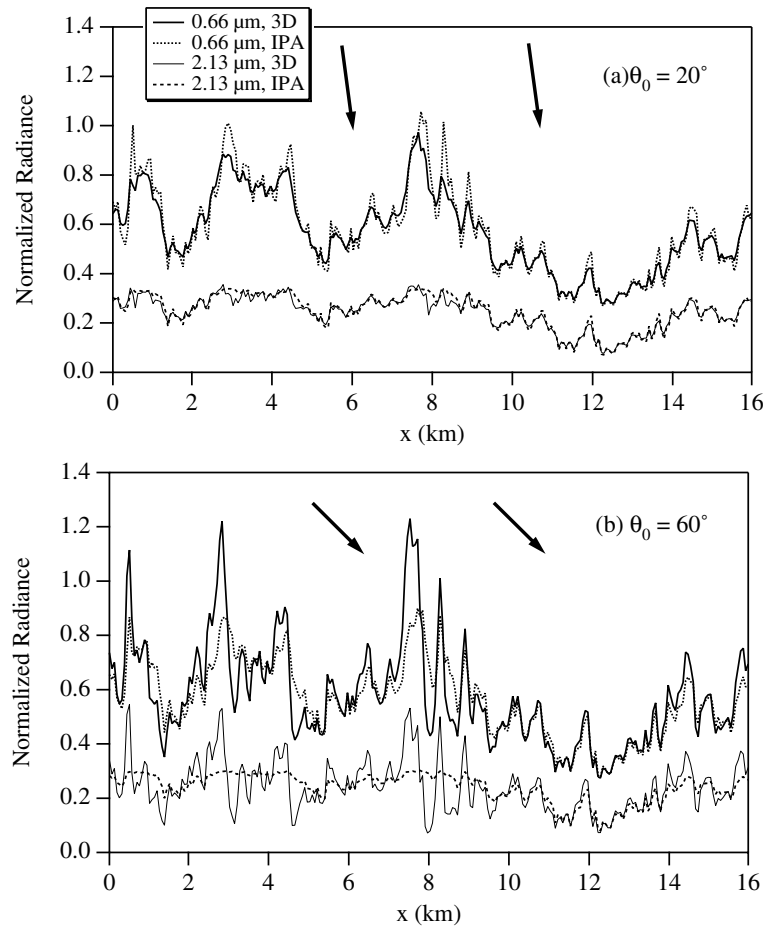
Fig. 3.3. High-resolution normalized nadir radiances simulated by the 3D radiative transfer model and the IPA. For clarity, radiances for visible wavelength ($0.66\,\mu$m) were shifted by 0.2. Vertical homogeneity of liquid water was assumed for the experiment. The effective droplet radius was fixed at $10\,\mu$m for the entire domain.

and Marshak, 2003). Smoothing dominates for visible wavelengths and is caused by horizontal divergence of multiply scattered photons; smoothing is therefore most effective in optically thick regions. In optically thin regions, R_{3D} is similar to R_{IPA}, i.e., IPA closely approximates the 3D radiance. Less smoothing occurs at near-infrared wavelengths. At low solar elevations, optically thick regions show enhanced roughening that is introduced by shadowing and illumination of direct and low-order scattering beams. At near-infrared wavelengths, R_{IPA} shows small variability in optically thick regions, but R_{3D} shows large fluctuations. However, shadowing has smaller effects in optically thin regions, which helps to explain why R_{3D} is approximately the same as R_{IPA} at both visible and near-infrared wavelengths.
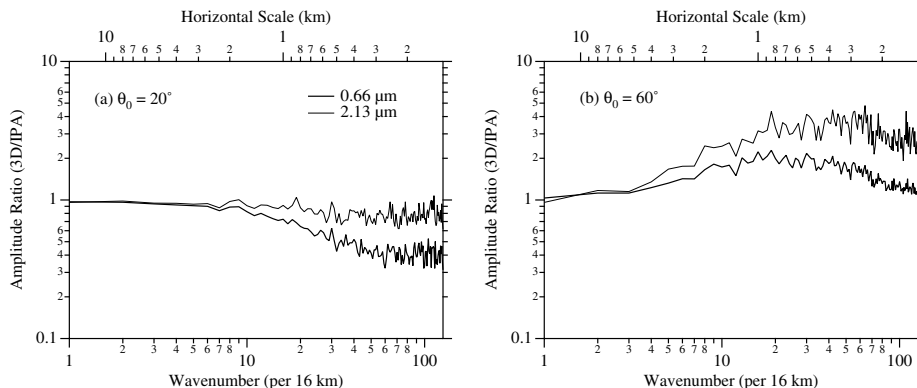
Fig. 3.4. Amplitude ratios of Fourier spectra of 3D radiance to those of IPA, at visible and near-infrared wavelengths.

The 3D radiative effects depend on the horizontal scale. This could be well known from power spectra of 3D and IPA radiances. Fig. 3.4 shows amplitude ratios of Fourier spectra between 3D and IPA nadir radiances. Each plot includes an ensemble average of ten cloud realizations. Amplitude ratios less than or greater than unity correspond to smoothing or roughening phenomena, respectively. At large horizontal scales (>5 km), the ratio is close to unity; IPA can approximate the 3D radiative transfer because net horizontal radiative transport can be neglected. At visible wavelengths, smoothing dominates for high solar elevations and small horizontal scales (<2 km), and roughening dominates for low solar elevations and intermediate horizontal scales (0.1–5 km). The 3D effects depend on the single scattering albedo (i.e., on wavelength and effective droplet radius). Less smoothing occurs for absorbing wavelengths (especially for larger effective radii). Thus, multi-spectral rather than single-spectral data can improve the retrieval accuracy of cloud parameters.

Fig. 3.5 shows amplitude ratios of visible-wavelength nadir radiances for values of $M = 0.5$, 1, and 1.5 with fixed inhomogeneity $V = 0.07$. The corresponding domain-averaged optical thicknesses are 3.9, 12, and 39, respectively, for each case. The geometric thickness given by (3.3) increases for increasing M, although the geometric roughness of the cloud top and bottom remains constant for fixed values of V. Smoothing is effective for moderate optical thickness at $M = 1$ but does not strongly depend on M. When the solar elevation is low, roughening is very sharp for optically thick clouds because shadowing and illumination of direct and forward-scattering beams are more effective for optically and geometrically thicker clouds. The amplitude of 3D radiance for $M = 1.5$ is four times the IPA radiance at horizontal scales of approximately 0.5–1 km. The 3D radiative effects thus vary substantially with mean optical thickness. The dependence of 3D effects on M at near-infrared wavelengths is similar to that at visible wavelengths (not shown).
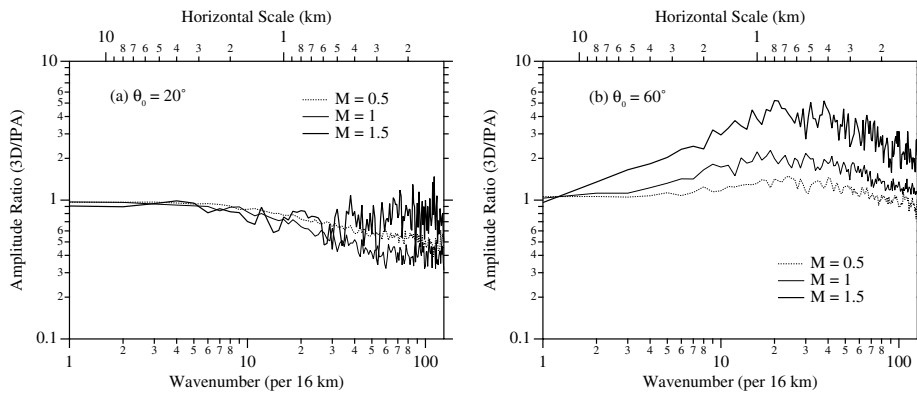
Fig. 3.5. Amplitude ratios of the Fourier spectra of 3D radiance to those of IPA, for various averaged logarithms of optical thickness, M, with a fixed inhomogeneity parameter, $V = 0.07$. Results are shown for visible wavelength ($0.66\,\mu m$).

Fig. 3.6 is the same as Fig. 3.5, but with $V = 0.03$, 0.07, and 0.11 for a fixed $M = 1$; corresponding domain-averaged optical thicknesses are 11, 12, and 14, respectively. No significant difference exists between the three cases because the effects of smoothing and roughening are independent of the inhomogeneity parameter V if M is the same. The inhomogeneity parameter roughly determines the amplitude of the IPA radiance fluctuation. Relative changes in the amplitude of the 3D radiance depend on the horizontal scale, wavelength, and cloud optical thickness, but not on horizontal inhomogeneity. If, for example, the 3D radiance for an inhomogeneous cloud field exhibits five-times smoother (or rougher) fluctuation than the IPA radiance, then that is also true for more homogeneous cloud field. Such a similarity of 3D radiative effects can be found between inhomogeneous and relatively homogeneous cloud fields. The 3D radiation problem and remote sensing retrieval algorithms can be simplified based on the similarity of 3D radiative effects related to inhomogeneity.
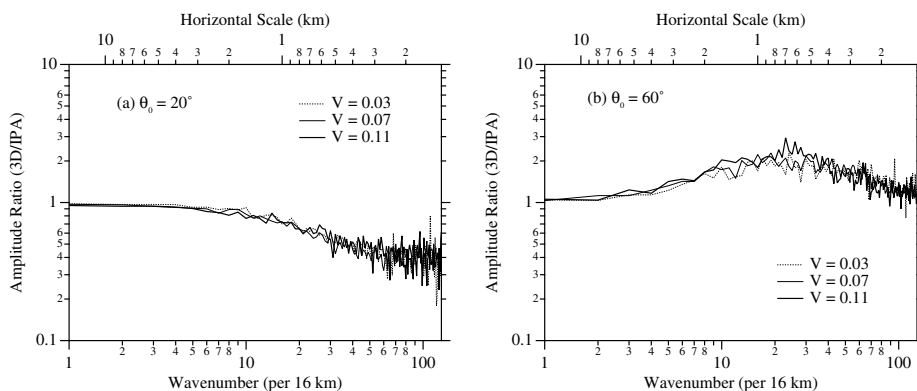

Fig. 3.6. As in Fig. 3.5, but for various values of V, with M fixed at 1.

3.4 Statistical analysis of the 3D effects and correction

This section describes the use of visible reflected radiance data with 1-km resolution to evaluate 3D effects on moments of cloud optical thickness retrievals. Optical thickness is often retrieved using only visible data because visible radiance is not highly dependent on the effective droplet radius. Results are shown for a wavelength of $0.64\,\mu$m that is the center of the Advanced Very High Resolution Radiometer (AVHRR) visible channel. The statistical quantities of the retrieved cloud optical thickness in the $8 \times 8\,\mathrm{km}^2$ domain were investigated. The goal was to correct the statistical properties of optical thickness retrieved with the IPA.

3.4.1 The influence on the statistics of retrieved optical thickness

The reflected radiance is roughly linear in $\log\tau$ especially when τ is between 3 and 30. When net horizontal radiative transport is absent, i.e., when the IPA works perfectly, moments of radiance are closely associated with moments of $\log\tau$ rather than moments of τ. Consider the mean and variance, M and V, respectively, of $\log\tau$. The pixel-average radiance of the IPA (R_{IPA}) is roughly approximated as the 1D radiance for PPH cloud with $\log\tau = M$, i.e.,

$$R_{\mathrm{IPA}} \sim R_{\mathrm{1D}}(\log\tau = M)\,. \tag{3.4}$$

This is equivalent to the effective thickness approximation of Cahalan et al. (1994a), who used it in calculating domain-averaged albedo. To improve the linear relationship, the following function can be used instead of $\log\tau$:

$$\chi = \frac{\gamma\tau}{1 + \gamma\tau}\,,$$

where the constant γ is $1-g$ (g is the asymmetry parameter and is approximately 0.86 for water clouds in the visible). However, this paper is devoted to analyses of mean and variance of $\log\tau$ for simplicity.

A cloud field can be characterized by the two statistical quantities, M and V. If conventional IPA inversion is used to retrieve the optical thickness from satellite measurements, then the retrieved value is biased because 3D radiative effects influence the observed radiance. Here, M_{IPA} and V_{IPA} are the mean and variance, respectively, of the logarithm of retrieved optical thickness. Fig. 3.7 shows the frequency distribution of initial and retrieved optical thickness for a cloud field with inhomogeneity $V = 0.09$ for the $8 \times 8\,\mathrm{km}^2$ region. The initial field of the optical thickness was artificially generated using the cloud model (section 3.2). For this field, 3D radiances were simulated and subsequently used to retrieve the optical thickness with the IPA inversion. Thus, we can estimate the error in the retrieved value by comparing with the initial (truth) data. It is shown that both M_{IPA} and V_{IPA} are biased, with the biases defined as

$$\Delta M \equiv M_{\mathrm{IPA}} - M \tag{3.5a}$$

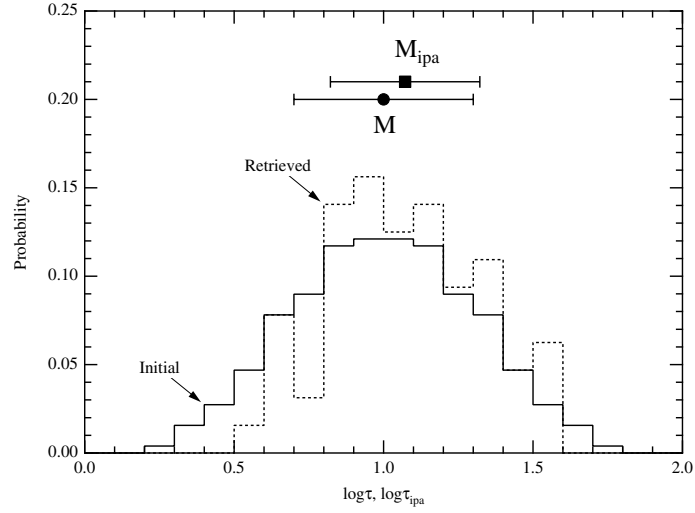$$\Delta V \equiv V_{\mathrm{IPA}} - V\,. \tag{3.5b}$$

Fig. 3.7. Frequency distributions of initial optical thickness ((τ) and retrieved optical thickness (τ_{IPA}) for an inhomogeneous cloud field. Marks in the upper part denote mean values of $\log \tau$ (circles) and $\log \tau_{ipa}$ (squares), and bars correspond to respective standard deviations. This example is for a case of backscattering viewing geometry ($\theta_0 = 60°$, $\mu = 0.7$–0.8, $\phi = 150°$–$180°$).

These biases imply differences between statistical properties of 3D radiance and IPA radiance. For a homogeneous cloud field, both biases should be zero because the 1D radiative transfer can accurately approximate the observed radiance. Biases will be large for inhomogeneous cloud fields.

3.4.2 Biases in the statistics of the optical thickness

Biases in M_{IPA} and V_{IPA} were investigated under various boundary layer cloud conditions. Fig. 3.8 relates the biases with the viewing angle for four cloud models with different assumptions in geometric roughness. Results are shown for angular averages of radiance for bins of $\mu = \cos\theta$ (θ is viewing zenith angle) and relative azimuth angle, which is 0°–30° or 150°–180°. The angular averaging does not significantly affect this kind of results because the radiances were calculated at the level of highest cloud top and the spatial resolution being considered here is as low as 1 km. The bias in M_{IPA} has small negative values for an overhead sun (the solar zenith angle $\theta_0 = 0°$). This bias is ascribed to the tilted cloud surface that reflects photons in the off-nadir direction and leads to the decrease of the near-nadir reflection. For an oblique sun ($\theta_0 = 60°$), the bias in M_{IPA} is negative for the forward view due to cloud side shadowing and positive for the backward view due to cloud side illumination. The tendency of the cloud 3D effect is similar among the four cloud models, but its magnitude differs substantially and increases for clouds with rough tops. Cloud top bumps allow for large horizontal transport of incident and reflected solar radiation. In addi-
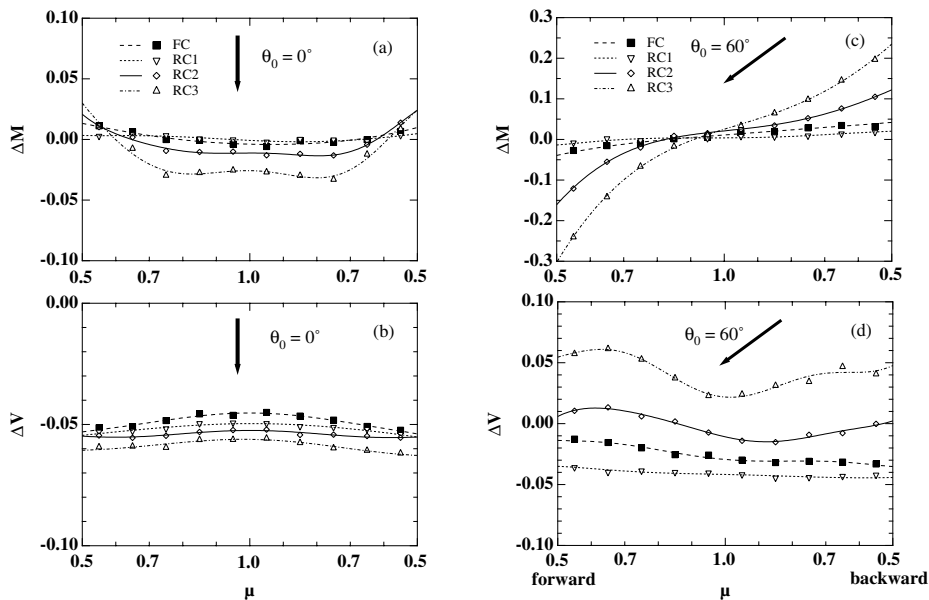
Fig. 3.8. The biases ΔM (a) and (c) and ΔV (b) and (d) as functions of cosine of viewing zenith angle ($\mu = \cos\theta$), for four cloud models: flat cloud (FC), cloud with a rough bottom and flat top (RC1), cloud with a rough top and bottom (RC2), and cloud with a flat bottom and rough top (RC3). The domain-averaged geometric thickness and the local optical thickness of each column are the same for the four models. Results are shown for angular averages of radiance for bins of μ and the relative azimuth angle (ϕ), which is $0°$–$30°$ for the left hand side of each panel or $150°$–$180°$ for the right hand side.

tion, most of the photons are reflected from the upper part of the cloud layer, so that cloud top inhomogeneity is important. Many observations of boundary layer clouds using lidar, radar, and stereo-photography have shown rough cloud tops and cloud bottoms (e.g., Boers et al., 1998; Kikuchi et al., 1993; Vali et al., 1998). Such an assumption therefore is reasonable in evaluating the 3D effects.

Fig. 3.8 also shows bias in the IPA-based retrieved inhomogeneity (V_{IPA}). Bias in V_{IPA} is large and negative when the solar elevation is high, which indicates that the spatial variability of the reflected radiance is small because of smoothing by photon diffusion in multiple scattering processes, as shown in section 3.3. An enhanced smoothing effect occurs in the model that includes bumpy cloud tops, which allow greater horizontal radiative transport than flat cloud tops. When the solar elevation is low, the opposite effect, roughening, is caused by enhanced variability of direct and low-order scattering of radiation incident to the inhomogeneous cloud column. The roughening effect is large for bumpy cloud tops and closely associated with the cloud top structure. Figure 3.8 (d) shows a tendency for sharper roughening in the forward view than in the backward view. Both bright and dark regions of the cloud surface are viewed in the for-

ward view; direct solar beams illuminate the bright regions, and optically dense parts shadow the dark regions. However, bright parts are mainly viewed in the backward direction, which decreases the reflectance contrast.

The viewing angle dependence of the 3D effect suggests that satellite-derived optical thickness is systematically larger for backward views than for forward views. Loeb and Coakley (1998) reported a systematic decrease in observed optical thickness with increasing viewing angle in the forward view, results that are consistent with results presented here. Similarly, Oreopoulos and Davies (1998a) showed a solar zenith angle dependence on the variance of $\log \tau_{\mathrm{IPA}}$ that was remotely sensed using AVHRR data. In their results, the variance of $\log \tau_{\mathrm{IPA}}$ systematically increased as the solar zenith angle increased between $\theta_0 = 50°$–$80°$, results that are consistent with the results presented here.

Figure 3.9 compares ΔM and ΔV to the inhomogeneity parameter V. Large values of V are associated with large variability in optical and geometrical thicknesses and the cloud top height. The standard deviation of the cloud top height is large for a large V. The absolute value of ΔM increases as V increases so that cloud 3D effects on brightness (e.g., brightening and darkening) are governed by the parameter V. In fact, ΔM is nearly proportional to V. The parameter V is important in describing the radiative effects of cloud inhomogeneity. In addition, ΔV is roughly proportional to V, and the proportionality is good except for off-nadir views with oblique sun. In other words, the relative bias $\Delta V/V$ is nearly constant with respect to the bi-directional angle. Thus, smoothing and roughening phenomena are almost independent of the degree of horizontal inhomogeneity and the two-parameter representation (with M and V) simplifies the 3D radiative effect dependence on the degree of inhomogeneity.
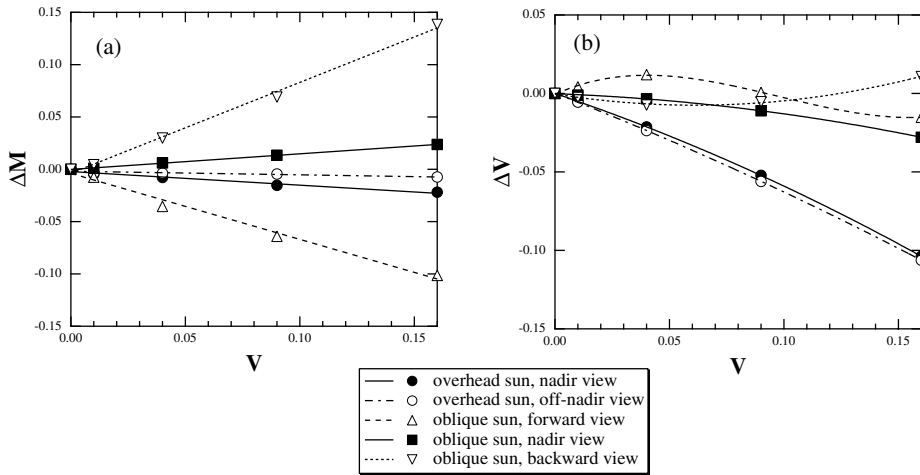

Fig. 3.9. IPA biases (a) ΔM and (b) ΔV as functions of the inhomogeneity parameter V for overhead sun ($\theta_0 = 0°$) and oblique sun ($\theta_0 = 60°$). Geometric parameters are 'nadir view,' $\mu = 0.9$–1.0, $\phi = 0°$–$30°$; 'off-nadir view,' $\mu = 0.6$–0.7, $\phi = 0°$–$30°$; 'forward view,' $\mu = 0.6$–0.7, $\phi = 0°$–$30°$; 'forward view,' $\mu = 0.6$–0.7, $\phi = 150°$–$180°$.

Legend:
— ● overhead sun, nadir view
—·— ○ overhead sun, off-nadir view
--- △ oblique sun, forward view
— ■ oblique sun, nadir view
······ ▽ oblique sun, backward view
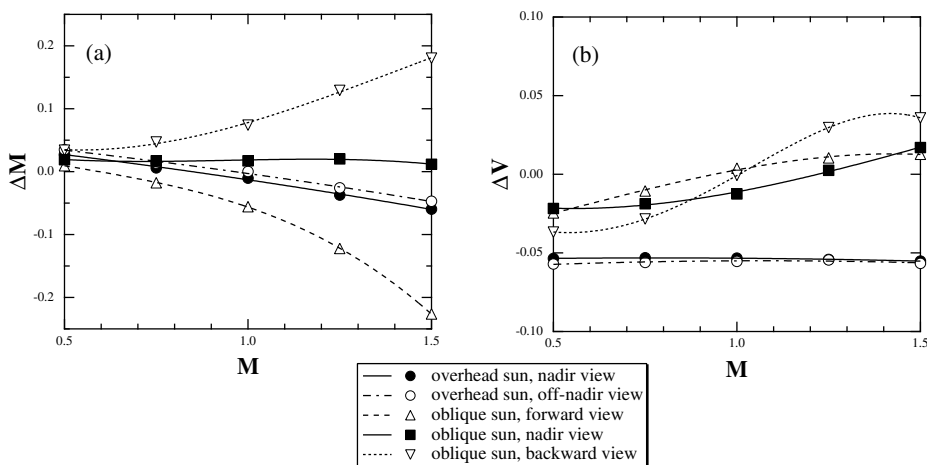
Fig. 3.10. As in Fig. 3.7, but for a function of M.

Fig. 3.10 compares ΔM and ΔV to M. A high sensitivity of ΔM to M is obvious, especially for off-nadir views with oblique sun. The difference in ΔM between the forward and backward views increases for optically thick cloud fields. The 3D effects on brightness are sharp for optically thick cloud fields. The bias ΔV increases with increasing M for oblique sun but is almost independent of M for overhead sun, because the roughening is sharp for optically thick clouds, as shown in Fig. 3.5. In thick clouds, photons travel short trajectories (on average). Thus the horizontal distance between the incident point at the cloud surface and the reflected exit point is relatively close, reducing the smoothing effect.

The solar zenith angle dependence of the IPA-retrieved optical thickness may be the most remarkable artifact of neglecting 3D effects. The average of the retrieved optical thickness can be roughly estimated as

$$\log \bar{\tau}_{\mathrm{IPA}} \cong M_{\mathrm{IPA}} + \frac{\ln 10}{2} V_{\mathrm{IPA}} .$$

Figure 3.11 shows angular distributions for a typical case with $M = 1$ and $V = 0.09$. For this case, the above equation for nadir-viewing geometry ($\mu = 1$) yields estimated mean optical thicknesses of 11, 13, and 17, respectively, for $\theta_0 = 0°$, $60°$, $70°$. The true mean optical thickness is 12.7. Such a solar angle dependence could appear in cloud climatology. For example, the annual zonal-mean optical thickness of low clouds increases with increasing latitude from about 5 at the Equator to about 12 at $60°$ north and south in the International Satellite Cloud Climatology Project (ISCCP) product (Tselioudis et al., 1992; Drake, 1993). Seasonal changes have also been reported. Latitudinal and seasonal changes might be partly affected by 3D effects. Therefore, global observations of the inhomogeneity parameter and correction of the IPA retrieved optical thickness to account for 3D radiative effects are clearly warranted.
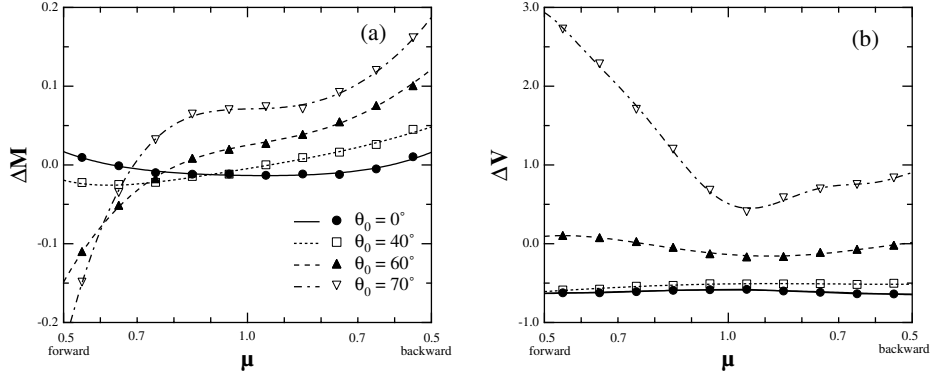
Fig. 3.11. Viewing angle distributions of the IPA biases ΔM and ΔV for the four solar zenith angles $\theta_0 = 0°$, $40°$, $60°$, $70°$.

3.4.3 Bias removal

To correct for the 3D effect on retrieved optical thickness, some empirical assumptions are required because it is difficult to retrieve several properties of clouds from optical remote sensing (e.g., cloud top roughness at sub-pixel scales). If the vertical profile of liquid water is prescribed (e.g., as the adiabatic parcel) and geometrical parameters (thickness and cloud top/bottom hight) are assumed to link to the optical thickness solely, then biases in the mean and variance of the logarithm of retrieved optical thickness can be expressed as

$$\frac{\Delta M}{V} = f(\mu_0, \mu, \phi; M, \alpha_g) \tag{3.6a}$$

$$\frac{\Delta V}{V} = g(\mu_0, \mu, \phi; M, \alpha_g) \tag{3.6b}$$

where μ_0 and μ are cosines of solar and satellite zenith angles, respectively, and α_g is the surface albedo. The proportionality of the biases to the inhomogeneity parameter V in (3.6) simplifies the parameterization. The formulation could be further modified to include additional minor factors including the relationship between optical and geometrical thickness in cloudy columns, vertical inhomogeneity in columns, effective particle radius, and azimuth-dependent orientation of cloud inhomogeneity. The functions f and g can be tabulated and computed by interpolation using a look-up table. Such computations are better than the function fitting shown by Iwabuchi and Hayasaka (2002).

Equations (3.5) and (3.6) can easily be applied to correct the retrieved optical thickness from satellite observations. They form a nonlinear system of equations for M and V that can be solved by the method of iterations:

(i)   Initial estimates: $M = M_{IPA}$, $V = V_{IPA}$
(ii) Biases ΔM, ΔV computed using (3.6)
(iii) Biases removed: $M = M_{IPA} - \Delta M$, $V = V_{IPA} - \Delta V$
(iv) If results have converged, then end. Otherwise, return to step (ii)

If needed, the mean and standard deviation of the optical thickness can be estimated as a by-product from M and V, using Eqs. (3.2a) and (3.2b). If the statistics of τ are more important than those of $\log\tau$, then a parameterization of the bias in the statistics of τ can be developed, with a form similar to that of (3.6). A main advantage of this type of correction method is that it can be used after conventional IPA retrieval; no reanalysis that uses the radiance is required. The above algorithm corrects the statistics; however, pixel optical thickness could be corrected following a similar path. After the corrected statistics M and V are computed, pixel optical thickness can be estimated by

$$\log\tau = M + \sqrt{\frac{V}{V_{\mathrm{IPA}}}}\left(\log\tau_{\mathrm{IPA}} - M_{\mathrm{IPA}}\right) \tag{3.7}$$

This algorithm may be useful for correcting any operational product currently derived using IPA.

Another possible method is to use a parameterization of the statistics of radiances. Differences in the average and variance of the 3D radiance from that of IPA radiance can be expressed as

$$\bar{R}_{\mathrm{3D}} - \bar{R}_{\mathrm{IPA}} = f'(\mu_0, \mu, \phi; M, V, \alpha_g) \tag{3.8a}$$

$$\sigma_{\mathrm{3D}}^2 - \sigma_{\mathrm{IPA}}^2 = g'(\mu_0, \mu, \phi; M, V, \alpha_g) \tag{3.8b}$$

The retrieval algorithm first corrects the observed (3D) radiance and then estimates the IPA radiance using the parameterization. Then, optical thickness (or its moments) can be estimated from the IPA radiance. This algorithm does require analyses of observed radiances and cannot be used to correct operational products.

3.5 Pixel-by-pixel retrieval

Pixel-by-pixel retrievals of the pixel-averaged optical thickness and droplet effective radius are discussed in this section. These two parameters are usually retrieved with the IPA; the parameters are inverted from observed visible and near-infrared radiances and theoretical simulations that use a 1D radiative transfer model (Fig. 3.12). The use of data with resolution of 250 m (i.e., the same resolution as for MODIS visible channels) is considered first. The target spectral wavelengths in this study were 0.66 and 2.13 μm, which are the center wavelengths of visible and near-infrared MODIS bands, respectively.

Figure 3.1 shows that the 3D radiance is poorly associated with local cloud properties, mainly because 3D radiance can be affected by net horizontal radiative transport from neighboring pixels. Unfortunately, the quantity observed is the 3D radiance rather than the IPA radiance. Once multi-spectral IPA radiances are estimated, optical thickness and effective radius can be retrieved conventionally by interpolation from a look-up table (Fig. 3.12). Thus, retrieval of inhomogeneous cloud parameters can be restated regarding how to estimate
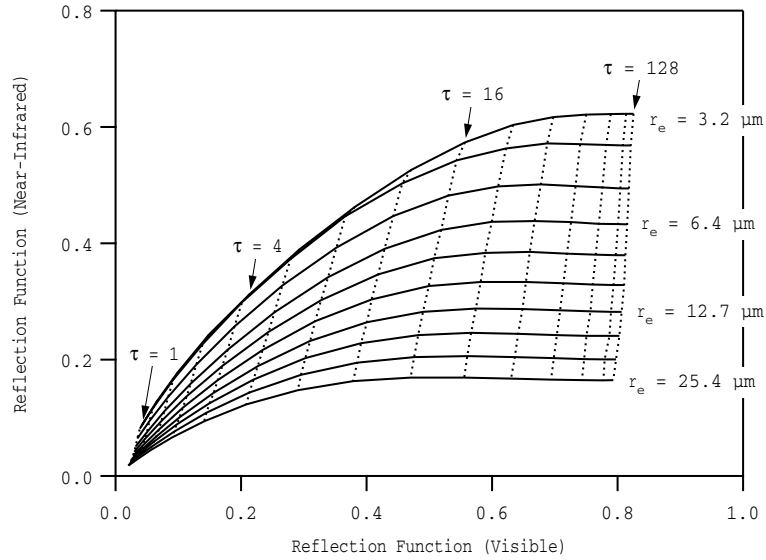
Fig. 3.12. Relationships between cloud parameters (optical thickness and effective particle radius) and reflection functions simulated by the 1D radiative transfer model for plane-parallel clouds.

the IPA radiance from (observed) 3D radiance. Therefore, neighboring pixel data are used to estimate the IPA radiance, which has a one-to-one relationship with the cloud property. This is the basis of non-local retrieval methods such as NIPA (Marshak et al., 1998). One can consider an alternative approach, as shown in section 3.5.4; if the 3D radiance can be estimated from IPA radiance using some method, then that method can also be used to retrieve cloud parameters.

The 3D-to-IPA estimate or IPA-to-3D estimate can be done using a convolution (or filtering). Estimated radiance is then a summation of all contributions from adjacent pixels. This technique is so flexible that a filter can be designed to treat 3D radiative effects, which work differently by solar zenith angle, average optical thickness, single scattering albedo that depends on wavelength and effective particle radius, as shown in section 3.3. An empirical model can be used to determine the filter; this model could be based on regressions using the least-squares method, neural nets, genetic algorithms, or a Bayesian method.

3.5.1 Retrieval method using adjacent pixel information

In the method presented here, multi-spectral IPA radiances were estimated from observed radiances at target and neighboring pixels within 750 m of the target, using a technique similar to a convolution. The coefficients for the convolution kernel can be determined by a regression that uses 3D radiances simulated under various conditions (e.g., average optical thickness and effective radius).

The IPA radiances Y that depend strongly on the physical quantities (i.e. optical thickness and effective radius) of the target pixel are represented in the

following regression formula:

$$
\begin{aligned}
Y \;=\; a + \sum_{i=1}^{m} \Bigg\{ & b_i \tilde{X}_i + \sum_{j=-n}^{-1} c_{ij} \frac{X_{i,j} - X_{i,j+1}}{\tilde{X}_i} + c_{i0}(X_{i,0} - \tilde{X}_i) \\
& + \sum_{j=1}^{n} c_{ij} \frac{X_{i,j} - X_{i,j+1}}{\tilde{X}_i} \Bigg\}
\end{aligned} \tag{3.9}
$$

where $m = 2$, $X_{i,j}$ denotes a 3D radiation function at the ith wavelength and the jth pixel, $\tilde{X}_i$ is the averaged 3D radiation function over j from $-n$ to n, and a, b_i, and c_{ij} are coefficients. The pixel index j is 0 for the target pixel; $j < 0$ and $j > 0$ denote neighboring pixels. The number of neighboring pixels was set to $n = 3$, and data from pixels within $750\,\mathrm{m}$ of the target pixel were used. Preliminary tests showed that neighboring pixels beyond $n = 3$ did not significantly improve the retrieval accuracy. Table 3.1 summarizes definitions adopted for Y and the corresponding $X_{i,j}$. Coefficients and 3D radiative functions ($X_{i,j}$) are defined independently for respective IPA radiances (visible and near-infrared), as in Table 3.1. Once the IPA radiances are estimated from observed 3D radiation functions ($X_{i,j}$) using the above equations, cloud properties can be retrieved conventionally from the one-to-one relationship between IPA radiances and cloud properties using a lookup table and interpolation as in Fig. 3.12.

Table 3.1. Radiative quantities used for the regression model of Eq. (3.9)

Y	$X_{1,j}$	$X_{2,j}$
$R_{\mathrm{ipa}}(\lambda = 0.66, \tau, r_{\mathrm{e}})$	$R_{\mathrm{3d}}(\lambda = 0.66, j)$	$R_{\mathrm{3d}}(\lambda = 0.66, j)/R_{\mathrm{3d}}(\lambda = 0.66, j)$
$R_{\mathrm{ipa}}(\lambda = 2.13, \tau, r_{\mathrm{e}})$	$R_{\mathrm{3d}}(\lambda = 2.13, j)$	$R_{\mathrm{3d}}(\lambda = 2.13, j)/R_{\mathrm{3d}}(\lambda = 0.66, j)$

The coefficients, a, b_i, and c_{ij}, were determined using the least-squares method. The regression used training data sets of IPA and 3D radiances for several cloud realizations. One set of coefficients was determined for R_{ipa} for each wavelength and for each solar and view directions. The estimation formula (3.9) was used to recover information lost by the 3D radiative effects including radiative smoothing and shadowing. Faure et al. (2002) showed that a de-smoothing process such as image enhancement is required for smoothed data. In addition, smoothing should operate in the solar azimuth direction for data roughened by the shadowing that works in that direction. The horizontal distributions of the coefficients c_{ij} can be considered as a filter that operates on 3D radiance data. Section 3.3 showed that radiative smoothing and roughening work differently for average optical thickness and effective particle radius. Different sets of regression coefficients were therefore prepared for different average optical thickness and effective particle radius values.

The method described above can be simplified to a method that uses single-spectral and/or local data. If local data are used to estimate the IPA radiance,

then $n = 0$, and equation (3.9) becomes

$$Y = a + \sum_{i=1}^{m} b_i X_{i,0} \,. \tag{3.10}$$

Similarly, a method might use single-spectral visible radiance to retrieve optical thickness. The next sections investigate performances of the single-spectral local (SSL) retrieval method, the single-spectral non-local (SSN) method, and the multi-spectral local (MSL) method. Tables 3.2 and 3.3 summarize data used in the five methods, including IPA.

Table 3.2. Numbers of spectral wavelengths (m) and neighboring pixels ($2n$) used to retrieve cloud optical thickness

Method	m	n
IPA	1 (*)	0
SSL	1 (*)	0
SSN	1 (*)	3
MSL	2	0
MSN	2	3

Independent pixel approximation (IPA), single-spectral local (SSL), single-spectral non-local (SSN), multi-spectral local (MSL), and multi-spectral non-local (MSN) methods. (*) Visible wavelength data were used.

Table 3.3. Number of spectral wavelengths (m) and neighboring pixels ($2n$) used for two-parameter retrieval of cloud optical thickness and effective droplet radius

Method	m	n
IPA	2	0
MSL	2	0
MSN	2	3

Notation as in Table 3.2

3.5.2 Optical thickness retrieval

The performances of different methods of retrieving optical thickness are compared. Table 3.2 lists the five methods: IPA, SSL, SSN, MSL, and MSN. Cloud realizations were generated with the domain average optical thickness of 12 and standard deviation of 8. Quasi-observation radiances were simulated with a stochastic cloud model and a 3D radiation model. Such radiances are used to assess retrieval algorithms. The retrieval error can be estimated by considering the input distribution of cloud parameters to be true.
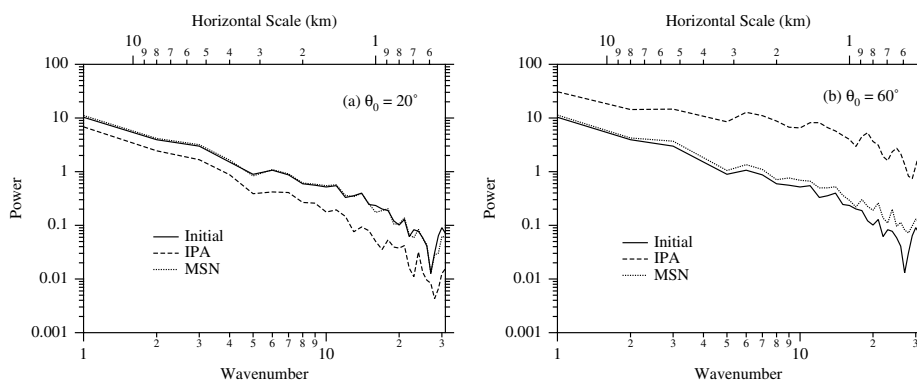
Fig. 3.13. Power spectra of the initial and retrieved optical thickness from the IPA and from the empirical retrieval method (MSN) that uses multi-spectral data and neighboring pixel data.

Figure 3.13 shows ensemble-average power spectra of the reference (initial) and retrieved pixel-averaged optical thickness. IPA-retrieved optical thickness is affected significantly by smoothing and roughening. In contrast, the MSN method almost perfectly reproduces the original fluctuations when the solar elevation is high. Even for low solar elevations, the MSN method retrieves a fluctuation, albeit rougher, that is very close to the original. Both multi-spectral data and neighboring pixel data improve the retrieval, as does the ability to incorporate filtering as used in image processing (e.g., image enhancement, phase correction, and smoothing).

Figure 3.14 shows the root mean square errors (RMSEs) for retrieved pixel-averaged optical thickness. The RMSE with IPA is 15–20% for $\theta_0 = 20°$ and 50–80% for $\theta_0 = 60°$. The SSL method uses the same data as the IPA method, but the SSL error is much smaller because the SSL method uses an empirical model that is based on 3D models. The retrieval performance of the SSN method is better than that of the MSL method in most cases, and both are better than the SSL method. Use of non-local data is particularly effective for high solar elevations. In addition, multi-spectral data reduce the retrieval error primarily at low solar elevations. The MSN method has the best performance. The RMSE is 4–6% for $\theta_0 = 20°$ and 7–8% for $\theta_0 = 60°$. Errors are smaller than in the IPA method by a factor of 3–10. The use of both multi-spectral and non-local data yields better estimates of cloud properties.

3.5.3 Retrieval of optical thickness and effective particle radius

Section 3.3 showed that 3D radiative effects depend primarily on average optical thickness and single scattering albedo (i.e., on effective radius). Therefore, regression coefficients in (3.9) were determined independently and tabulated for different combinations of average optical thickness and effective droplet radius. Regression coefficients vary strongly with the average optical thickness and effec-
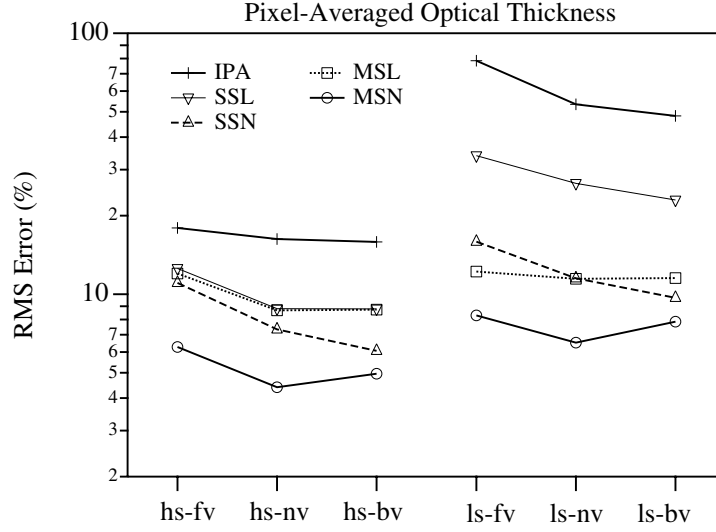
Fig. 3.14. Root-mean-square errors (RMSEs) in the retrieved optical thickness for various methods: IPA, single-spectral local (SSL), single-spectral non-local (SSN), multi-spectral local (MSL), multi-spectral non-local (MSN). Notations on the horizontal axis: 'hs': high solar elevation ($\theta_0 = 20°$); 'ls': low solar elevation ($\theta_0 = 60°$); 'fv': forward view; 'nv': nadir view; 'bv': backward view. For oblique views, the view zenith angle is $30°$; the relative azimuth angle is $0°$ and $180°$ for the forward and backward views, respectively.

tive radius. That variability underscores the importance of training for various cases to generalize the empirical model.

Retrieved cloud parameters vary according to what set of regression coefficients for specific averages of optical thickness and effective radius are used. However, accurate estimates of the averages are unavailable when the retrieval algorithm is initially applied. Thus, optimal values of pixel-averaged optical thickness ($\bar{\tau}$) and effective radius ($\bar{r}_{\mathrm{eff}}$) were derived using an iterative procedure that included three processes:

(i)   estimation of pixel averages, $\bar{\tau}$ and $\bar{r}_{\mathrm{eff}}$, from the IPA radiances that are derived using (3.9);

(ii) computation of running averages of cloud parameters within $750\,\mathrm{m}$ of the center of the target pixel;

(iii) computation of regression coefficients interpolated for the previously computed running averages.

A few iterations are usually sufficient to obtain a converged set of $\bar{\tau}$ and $\bar{r}_{\mathrm{eff}}$.

Figure 3.15 shows initial and retrieved cloud quantities from the IPA and MSN methods. Smoothing and roughening has a big influence on pixel-averaged optical thickness in the IPA method. Negative and positive mean biases exist for high and low solar elevations, respectively. The IPA error in $\bar{\tau}$ for $\bar{\tau} > 30$ is very large ($>100\%$) for low solar elevations. In addition, large positive error is present
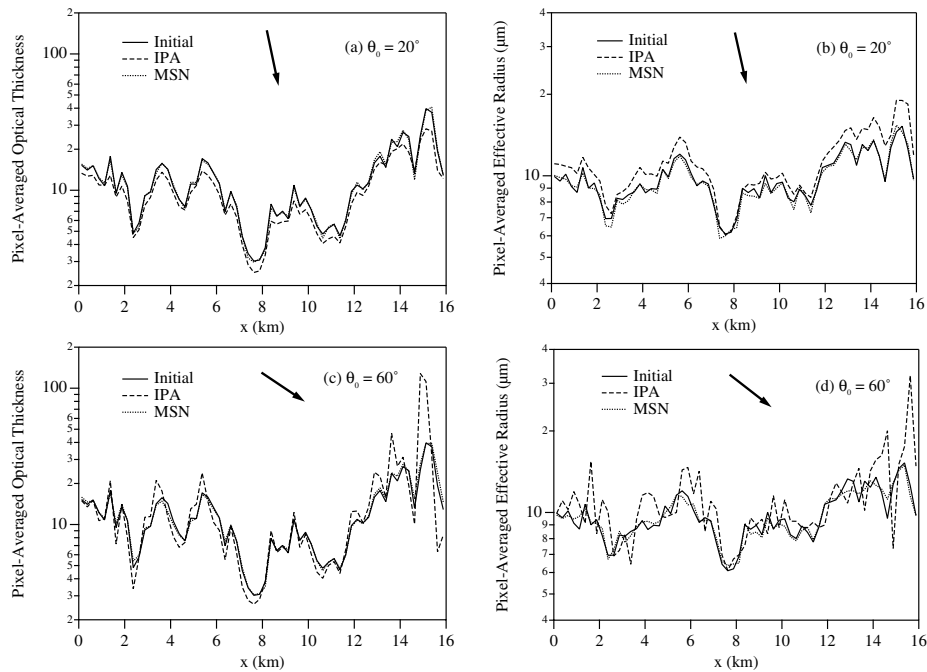
Fig. 3.15. Retrieved parameters from the IPA and MSN methods, and the initial distributions of (a) and (c) optical thickness and (b) and (d) effective radius. Retrieval simulations used 3D nadir radiances as virtually observed radiances.

at the sunny parts of clouds because of enhanced direct beam illumination. Large negative bias appears at shadowed sides. In contrast, the MSN method yields an optical thickness that is distributed closely around the initial value, with almost no mean bias. In addition, the MSN method successfully corrects a phase lag in optical thickness fluctuations when roughening occurs. The effective radius from the IPA method has positive bias for both solar angles, with a significant fluctuation for low solar elevations. In contrast, the MSN retrieval of effective radius is highly accurate, although accurate fluctuations at small horizontal scale are difficult to obtain even with the MSN method, especially for low solar elevations.

Figure 3.16 compares retrieval errors for the IPA, MSL, and MSN methods. The RMSE in optical thickness is similar to that in the previous case study (Fig. 3.14). The MSN method outperforms the other methods. The RMSE in the MSN method is smaller than in the IPA by a factor of 3 for $\theta_0 = 20°$ and 10 for $\theta_0 = 60°$. MSN error is about 50% of the MSL error. The relative error in effective radius with the IPA method is 15–25% and 30–40% for $\theta_0 = 20°$ and 60°, respectively. That error is reduced in the MSN method to 4–7% and 5–8%, respectively. The RMSE of the retrieved effective radius using MSN is similar to that from the MSL method when $\theta_0 = 20°$. However, the MSN error is three times smaller than the MSL error when the sun is low ($\theta_0 = 60°$). Retrieval errors
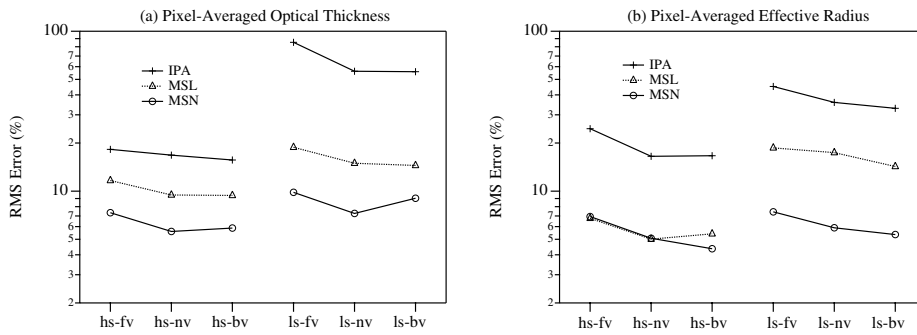
Fig. 3.16. As in Fig. 3.13, but for the retrieval of optical thickness and effective droplet radius.

for both the optical thickness and effective radius can be reduced significantly using the MSN method. Iwabuchi and Hayasaka (2003) assessed the influences of a few assumptions in the cloud modeling on the retrieval performance of the empirical inverse model. They found that the MSN method outperforms the IPA method, even given the uncertainties in the cloud modeling. In other words, some 3D radiative effects that vary with situations can be well modeled in the empirical inverse model.

3.5.4 Advanced method

The empirical model in the previous section estimates IPA radiance from observed (3D) radiances. In contrast, a model can be developed to calculate 3D radiances from the IPA radiances. This method can also be used to retrieve cloud parameters using an iterative procedure:

(i)   Initial estimates of IPA radiances are equated as the observed radiances.
(ii) 3D radiance is computed from the IPA radiance using the empirical model.
(iii) IPA radiance estimates are modified by comparing 3D radiances and observed radiances.
(iv) Test for convergence (the 3D radiances are the same as the observations). If true, then finish. Otherwise, return to step (ii).
(v)   Finally, cloud properties are inverted from the estimated IPA radiances.

Zinner et al. (2006) proposed a similar iterative algorithm for optical thickness retrieval, applying direct 3D radiative transfer calculations instead of step (ii) in the above. Although the 3D radiative transfer codes may be easily used in retrieval algorithms in the future, quicker calculation methods are preferable with currently limited computational power. In the IPA-to-3D conversion, a 2D filter convolution on the IPA radiances can be used. This idea is similar to one shown by Várnai and Marshak (2003). The filter expresses solar-azimuth dependence of contributions of horizontal radiative transport to the emergent radiance. The filter should be designed to include 3D radiative effects, such as

diffusion, direct beam effects, and other minor effects such as backscattering. Diffusion is assumed to work isotropically in all azimuth directions. Direct beam and backscattering effects operate along solar azimuths, and the horizontal scale length is a function of solar zenith angle. Filter coefficients were determined by the least-squares method under different cloud conditions and for different averages of optical thickness and effective radius. Radiative transfer simulations of visible and near-infrared wavelengths using the Monte Carlo radiation model were used to empirically determine the filter.

Figure 3.17 shows the approximately computed 3D radiance using the filter, at approximately 60-m pixel resolution. A horizontal segment along the solar azimuth was sampled from a 2D image and is shown in the figure. The radiance computed with filtering (filtered IPA, denoted as FIPA) is well correlated with the 3D radiance, suggesting that 3D radiative effects (such as shadowing and illumination) are well modeled by the empirical filter. FIPA accuracy is significantly higher than that of the method without filtering (i.e., just IPA). This is important because the performance of the IPA-to-3D conversion influences the retrieval performance in the inversion algorithm. Fig. 3.18 demonstrates parameter retrievals using FIPA and IPA. Significant retrieval error using IPA was absent for the FICA retrieval. The high-resolution data used (about 60 m) yields better estimates of cloud properties using a 2D filter that is adaptive to the solar azimuth of the case.
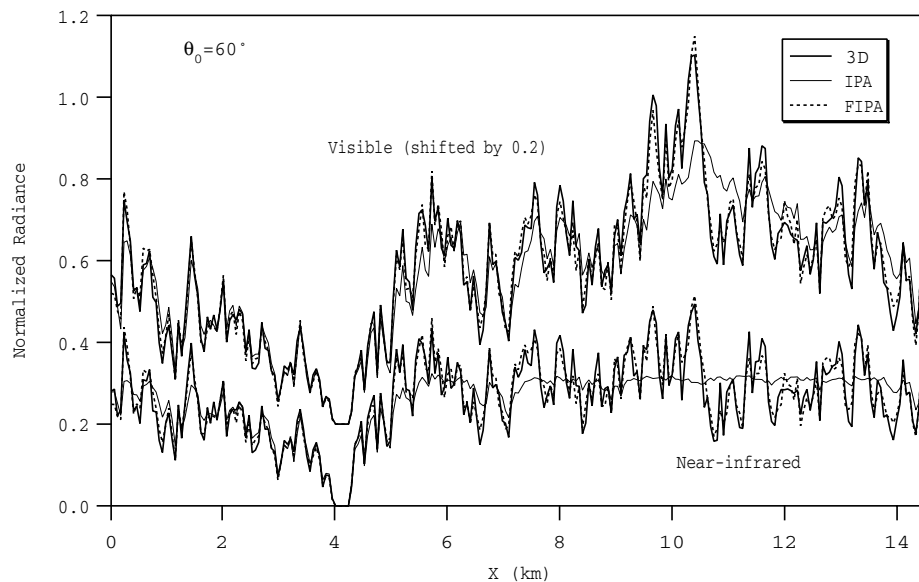

Fig. 3.17. Normalized nadir radiances computed by the 3D model, IPA, and by an empirical model that uses a filtering technique (FIPA), with approximately 60-m resolution.
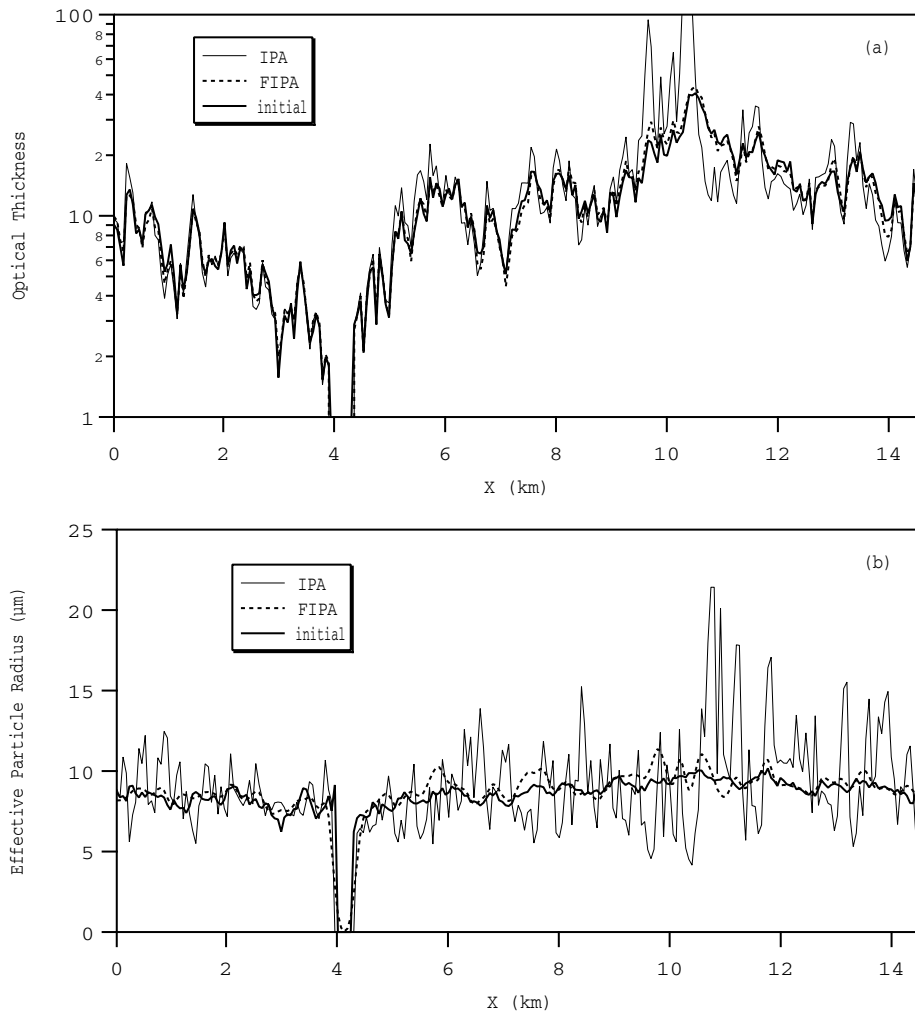
Fig. 3.18. Initial and retrieved cloud parameters. Retrieval simulations used the 3D radiances in Fig. 3.17 as virtually observed radiances.

3.6 Concluding remarks

The retrieval of optical thickness and effective radius in inhomogeneous clouds using satellite measurements has been considered. Several algorithms have been presented that yield improved estimates of cloud parameters by accounting for 3D radiative effects.

The first approach is a statistical correction of cloud parameters that are retrieved using 1D radiative transfer. We also examined the 3D radiative effects on the statistical quantities of optical thickness retrieved with independent pixel approximation (IPA) from visible-wavelength data with 1-km resolution.

Inhomogeneous clouds are characterized by two statistical quantities: the mean (M) and variance (V) of the logarithm of the optical thickness, where V represents a degree of horizontal inhomogeneity. These statistical quantities are most important in determining major 3D radiative effects on the optical thickness retrieval. The optical thickness retrieved with IPA was biased, and these biases in the moments were investigated. Retrieval of optical thickness is insufficiently accurate without cloud-top geometrical roughness information, especially for off-nadir views with oblique sun. Darkening of mean reflectance occurs for forward-scattering viewing geometry because of cloud side shadowing. Similarly, brightening occurs for back-scattering-view geometry because of cloud side illumination. Therefore, optical thickness retrieval should be restricted to close-nadir-view geometry if conventional IPA is applied to oblique sun angles. The effects of radiative smoothing and roughening dominate for overhead sun and oblique sun, respectively. This change in dominance may yield an apparent solar zenith angle dependence in the cloud inhomogeneity parameter estimated from the IPA-based retrieval. Solar angle dependence may produce an unrealistic latitudinal and seasonal dependence of optical thickness in cloud climatologies. A correction for the influence of cloud horizontal inhomogeneity is therefore warranted. Pixel-by-pixel parameter estimates have errors for low-resolution data because sub-pixel information is missing in spite of the fact that the information is important for interpreting the pixel radiance. However, estimates of reasonable cloud parameter statistics are more important even if pixel-by-pixel estimates are not accurate. From this perspective, the correction method of moments is a good approach for remote sensing of inhomogeneous clouds.

The second approach considered pixel-by-pixel retrieval, increasing the data used for a retrieval. An empirical model can be used to retrieve pixel-averaged cloud optical thickness and effective droplet radius. IPA pixel radiances at visible and near-infrared wavelengths are expressed in the empirical model using regression formulae with respect to multi-spectral 3D radiances at the target pixel and neighboring pixels. Even for cloud optical thickness retrievals, which often use single-spectral visible wavelength data, multi-spectral and non-local data improved retrieval performance. Training was done under a variety of conditions (e.g., average optical thickness and effective radius) to generalize the retrieval method because 3D radiative effects vary significantly as conditions vary. The empirical inversion model performed significantly better than the IPA inversion. Although vertical cloudy columns were assumed in the cloud modeling, this type of algorithm will not predict accurate single pixel properties if shear is present in the cloud. However, the algorithm would be useful in correcting some artifacts that appear in the retrieved cloud parameters using the IPA.

Parameter retrieval that accounts for 3D effects is feasible if geometric and microphysical properties of target clouds are well modeled. The assumption of inhomogeneous clouds is obviously more realistic than the plane-parallel homogeneous assumption. Better realism results when assumptions for the geometric and microphysical properties of clouds are more sophisticated. Data from in situ observations or output from cloud/eddy resolving model simulations may be useful for this purpose. Cloud top roughness especially plays a major role in

determining 3D radiative effects (Loeb et al., 1998; Várnai and Davies, 1999). Improvements in assumptions used in the retrieval algorithm will allow more reasonable estimates of cloud properties to be obtained from satellite measurements.

References

Barker, H. W., and J. A. Davies, 1992: Cumulus cloud radiative properties and the characteristics of satellite radiance wavenumber spectra. *Remote Sens. Environ.*, **42**, 51–64.

Barker, H. W., and D. Liu, 1995: Inferring optical depth of broken clouds from Landsat data. *J. Climate*, **8**, 2620–2630.

Barker, H. W., 1996: Estimating cloud field albedo using one-dimensional series of optical depth. *J. Atmos. Sci.*, **53**, 2826–2836.

Boers, R., J. D. Spinhirne, and W. D. Hart, 1988: Lidar observations of the fine-scale variability of marine stratocumulus clouds. *J. Appl. Meteor.*, **27**, 797–810.

Bower, K. N., T. W. Choularton, J. Latham, J. Nelson, M. B. Baker, and J. Jensen, 1994: A parameterization of warm clouds for use in atmospheric general circulation models. *J. Atmos. Sci.*, **51**, 2722–2732.

Brenguiter, J.-L., H. Pawlowska, L. Schüller, R. Preusker, J. Fischer, and Y. Fouquart, 2000: Radiative properties of boundary layer clouds: Effective droplet radius versus number concentration. *J. Atmos. Sci.*, **57**, 803–821.

Cahalan, R. F., W. Ridgway, W. J. Wiscombe, T. L. Bell, and J. B. Snider, 1994a: The albedo of fractal stratocumulus clouds. *J. Atmos. Sci.*, **51**, 2434–2455.

Cahalan, R. F., W. Ridgway, and W. J. Wiscombe, 1994b: Independent pixel and Monte Carlo estimates of the stratocumulus albedo. *J. Atmos. Sci.*, **51**, 3776–3790.

Chambers, L. H., B. A. Wielicki, and K. F. Evans, 1997: Accuracy of the independent pixel approximation for satellite estimates of oceanic boundary layer cloud optical depth. *J. Geophys. Res.*, **102**, 1779–1794.

Davis, A. B., A. Marshak, R. F. Cahalan, and W. J. Wiscombe, 1997: The Landsat scale break in stratocumulus as a three-dimensional radiative transfer effect: Implications for cloud remote sensing. *J. Atmos. Sci.*, **54**, 241–260.

Drake, F., 1993: Global cloud cover and liquid water path from ISCCP C2 data. *Int. J. Climatol.*, **13**, 581–605.

Evans, 1993: Two-dimensional radiative transfer in cloudy atmosphere: The spherical harmonic spatial grid method. *J. Atmos. Sci.*, **50**, 3111–3124.

Faure, T., H. Isaka, and B. Guillemet, 2001: Neural network retrieval of cloud parameters of inhomogeneous and fractional clouds: Feasibility study. *Remote Sens. Environ.*, **77**, 123–138.

Faure, T., H. Isaka, and B. Guillemet, 2002: Neural network retrieval of cloud parameters from high-resolution multispectral radiometric data: A feasibility study. *Remote Sens. Environ.*, **80**, 285–296.

Han, Q., W. B. Rossow, and A. A. Lacis, 1994: Near-global survey of effective droplet radii in liquid water clouds using ISCCP data. *J. Climate*, **7**, 465–497.

Hayasaka, T., M. Kuji, and M. Tanaka, 1994: Air truth validation of cloud albedo estimated from NOAA advanced very high resolution radiometer data. *J. Geophys. Res.*, **99**, 18 685–18 693.

Iwabuchi, H., 2000: Effects of cloud horizontal inhomogeneity on optical remote sensing of cloud parameters. Doctor thesis, Tohoku University, Sendai, Japan, 104 pp.

Iwabuchi, H., and T. Hayasaka, 2002: Effects of cloud horizontal inhomogeneity on the optical thickness retrieved from moderate-resolution satellite data. *J. Atmos. Sci.*, **59**, 2227–2242.

Iwabuchi, H. and T. Hayasaka, 2003: A multi-spectral non-local method for retrieval of boundary layer cloud properties from optical remote sensing data. *Remote Sens. Environ.*, **88**, 294–308.

Iwabuchi, H., 2006: Efficient Monte Carlo methods for radiative transfer modeling. *J. Atmos. Sci.*, **63**, 2324–2339.

Kikuchi, K., Y. Asuma, T. Taniguchi, M. Kanno, M. Tanaka, T. Hayasaka, T. Takeda, and Y. Fujiyoshi, 1993: Structure and reflectance of winter maritime stratocumulus clouds. *J. Meteor. Soc. Japan*, **71**, 715–731.

Loeb, N. G., and J. A. Coakley, Jr, 1998: Inference of marine stratus cloud optical depth from satellite measurements: Does 1D theory apply? *J. Climate*, **11**, 215–233.

Loeb, N. G., T. Várnai, and D. M. Winker, 1998: Influence of subpixel-scale cloud-top structure on reflectances from overcast stratiform cloud layers. *J. Atmos. Sci.*, **55**, 2960–2973.

Marshak, A., A. Davis, W. J. Wiscombe, and R. F. Cahalan, 1995a: Radiative smoothing in fractal clouds. *J. Geophys. Res.*, **100**, 26 247–26 261.

Marshak, A., A. Davis, W. J. Wiscombe, and G. Titov, 1995b: The verisimilitude of the independent pixel approximation used in cloud remote sensing. *Remote Sens. Environ.*, **52**, 71–78.

Marshak, A., A. Davis, R. F. Cahalan, and W. J. Wiscombe, 1998: Nonlocal independent pixel approximation: Direct and inverse problem s. *IEEE Trans. Geosc. and Remote Sens.*, **36**, 192–205.

Marshak, A., A. B. Davis, W. J. Wiscombe, and R. F. Cahalan, 1999: Horizontal radiative fluxes in clouds and accuracy of the independent pixel approximation at absorbing wavelengths. *Geophys. Res. Lett.*, **26**, 1585–1588.

Marshak A., S. Platnick, T. Várnai, G. Wen, R. F. Cahalan, 2006: Impact of three-dimensional radiative effects on satellite retrievals of cloud droplet sizes. *J. Geophys. Res.*, **111**, D09207, doi:10.1029/2005JD006686.

Minnis, P., P. W. Heck, D. F. Young, C. W. Fairall, and J. B. Snider, 1992: Stratocumulus cloud properties derived from simultaneous satellite and island-based instrumentation during FIRE. *J. Appl. Meteor.*, **31**, 317–339.

Nakajima, T., and M. D. King, 1990: Determination of the optical thickness and effective particle radius of clouds from reflected solar radiation measurements. Part I: Theory. *J. Atmos. Sci.*, **47**, 1878–1893.

Nakajima, T. Y., and T. Nakajima, 1995: Wide-area determination of cloud microphysical properties from NOAA AVHRR measurements for FIRE and ASTEX regions. *J. Atmos. Sci.*, **52**, 4043–4059.

Oreopoulos, L., and R. Davies, 1998a: Plane parallel albedo biases from satellite observations. Part I: Dependence on resolution and other factors. *J. Climate*, **11**, 919–932.

Oreopoulos, L., and R. Davies, 1998b: Plane parallel albedo biases from satellite observations. Part II: Parameterizations for bias removal. *J. Climate*, **11**, 933–944.

Oreopoulos, L., A. Marshak, R. F. Cahalan, and G. Wen, 2000: Cloud three-dimensional effects evidenced in Landsat spatial power spectra and autocorrelation functions. *J. Geophys. Res.*, **105**, 14 777–14 788.

Radke, L. F., J. A. Coakley, and M. D. King, 1989: Direct and remote sensing observations of the effects of ships on clouds. *Science*, **246**, 1146–1149.

Rosenfeld, D., 2000: Suppression of rain and snow by urban and industrial air pollution. *Science*, **287**, 1793–1796.

Rossow, W. B., and R. A. Schiffer, 1991: ISCCP cloud data products. *Bull. Amer. Meteor. Soc.*, **72**, 2–20.

Szczap, F., H. Isaka, M. Saute, B. Guillemet, and Y. Gour, 2000: Inhomogeneity effects of 1D and 2D bounded cascade model clouds on their effective radiative properties. *Phys. Chem. Earth*, **25**, 83–89.

Titov, G. A., 1998: Radiative horizontal transport and absorption in stratocumulus clouds. *J. Atmos. Soc.*, **55**, 2549–2560.

Tselioudis, G., W. B. Rossow, and D. Rind, 1992: Global patterns of cloud optical thickness variation with temperature. *J. Climate*, **5**, 1484–1495.

Vali, G., R. D. Kelly, J. French, S. Haimov, and D. Leon, 1998: Finescale structure and microphysics of coastal stratus. *J. Atmos. Sci.*, **55**, 3540–3564.

Várnai, T., and R. Davies, 1999: Effects of cloud heterogeneities on shortwave radiation: Comparison of cloud-top variability and internal heterogeneity. *J. Atmos. Sci.*, **56**, 4206–4224.

Várnai T., A. Marshak, 2003: A method for analyzing how various parts of clouds influence each other's brightness. *J. Geophys. Res.*, **108** (D22), 4706, doi:10.1029/2003JD003561.

Zinner T., B. Mayer, M. Schröder, 2006: Determination of three-dimensional cloud structures from high-resolution radiance data. *J. Geophys. Res.*, **111**, D08204, doi:10.1029/2005JD006062.

Zuidema, P., and K. F. Evans, 1998: On the validity of the independent pixel approximation for boundary layer cloud observed during ASTEX. *J. Geophys. Res.*, **103**, 6059–6074.